Oil & Gas Science and Technology – Rev. IFP Energies nouvelles (2016) **71**, 47

DOI: 10.2516/ogst/2015044

Zn(II), Mn(II) and Sr(II) Behavior in a Natural Carbonate Reservoir System. Part I: Impact of Salinity, Initial pH and Initial Zn(II) Concentration in Atmospheric Conditions

B. Auffray[1], B. Garcia[1]*, C.-P. Lienemann[2], L. Sorbier[2] and A. Cerepi[3]

[1] IFP Energies nouvelles, 1 et 4 avenue de Bois Préau, 92852 Rueil-Malmaison - France
[2] IFP Energies nouvelles, Rond-point de l'échangeur de Solaize, BP 3, 69360 Solaize - France
[3] EA 4592 G&E, ENSEGID, Université de Bordeaux, 1 allée F. Daguin, 33607 Pessac Cedex - France
e-mail: baptiste.auffray@beicip.com - bruno.garcia@ifpen.fr
charles.lienemann@ifpen.fr - loic.sorbier@ifpen.fr - adrian.cerepi@ipb.fr

* Corresponding author

Abstract — *The sorption of inorganic elements on carbonate minerals is well known in strictly controlled conditions which limit the impact of other phenomena such as dissolution and/or precipitation. In this study, we evidence the behavior of Zn(II) (initially in solution) and two trace elements, Mn(II) and Sr(II) (released by carbonate dissolution) in the context of a leakage from a CO_2 storage site. The initial pH chosen are either equal to the pH of the water-CO_2 equilibrium (~ 2.98) or equal to the pH of the water-CO_2-calcite system (~ 4.8) in CO_2 storage conditions. From this initial influx of liquid, saturated or not with respect to calcite, the batch experiments evolve freely to their equilibrium, as it would occur in a natural context after a perturbation.*

The batch experiments are carried out on two natural carbonates (from Lavoux and St-Emilion) with $P_{CO_2} = 10^{-3.5}$ bar, with different initial conditions ($[Zn(II)]_i$ from 10^{-4} to 10^{-6} M, either with pure water or 100 g/L NaCl brine). The equilibrium regarding calcite dissolution is confirmed in all experiments, while the zinc sorption evidenced does not always correspond to the two-step mechanism described in the literature. A preferential sorption of about 10% of the concentration is evidenced for Mn(II) in aqueous experiments, while Sr(II) is more sorbed in saline conditions. This study also shows that this preferential sorption, depending on the salinity, is independent of the natural carbonate considered. Then, the simulations carried out with PHREEQC show that experiments and simulations match well concerning the equilibrium of dissolution and the sole zinc sorption, with log $K_{Zn(II)}$ ~ 2 in pure water and close to 4 in high salinity conditions. When the simulations were possible, the log K values for Mn(II) and Sr(II) were much different from those in the literature obtained by sorption in controlled conditions. It is shown that a new conceptual model regarding multiple Trace Elements (TE) sorption is required, to enable us to better understand the fate of contaminants in natural systems.

Résumé — **Comportement du Zn(II), Mn(II) et Sr(II) au sein d'un système réservoir carbonate naturel. Partie 1 : impact de la salinité, du pH initial et de la concentration en Zn(II) en conditions atmosphériques** — La sorption d'éléments inorganiques sur les minéraux carbonatés est bien connue

dans des conditions strictement contrôlées, limitant l'impact d'autres phénomènes tels que la dissolution et/ou précipitation. Dans cette étude, nous mettons en évidence le comportement de Zn(II) (initialement en solution) et deux éléments « traces », Mn(II) et Sr(II) (relargués au cours de la dissolution des carbonates) dans un contexte d'une fuite d'un site de stockage de CO_2. Le pH initial choisi est, soit égal au pH de l'équilibre eau-CO_2 (~ 2,98), soit égal au pH du système eau-CO_2-calcite (~ 4,8) et ce, dans des conditions de stockage de CO_2. De cet afflux initial de liquide saturé ou non par rapport à la calcite, les expériences en réacteurs fermés évoluent librement jusqu'à équilibre, telles que des conditions de contexte naturel après une perturbation.

Les expériences en réacteurs fermés sont effectuées sur deux carbonates naturels (Lavoux et St-Émilion) avec une pression $P_{CO_2} = 10^{-3,5}$ bar, et des conditions initiales différentes ($[Zn(II)]_i$ variant de 10^{-4} à 10^{-6} M, soit avec de l'eau pure ou en présence de 100 g/L de NaCl). L'équilibre en ce qui concerne la dissolution de la calcite est confirmé dans toutes les expériences, tandis que la sorption de zinc mise en évidence ne correspond pas toujours au mécanisme en deux étapes décrit dans la littérature. Une sorption préférentielle d'environ 10 % de la concentration est mise en évidence pour Mn(II) dans des expériences aqueuses, tandis que le Sr(II) est plus « sorbé » dans des conditions salines. Cette étude montre également que cette sorption préférentielle, en fonction de la salinité, est indépendante du carbonate naturel considéré.

Les simulations effectuées avec PHREEQC montrent une bonne adéquation entre les expériences et les simulations concernant l'équilibre de dissolution et la seule sorption de zinc, avec un log $K_{Zn(II)} \sim 2$ dans l'eau pure et proche de 4 dans des conditions de haute salinité. Lorsque les simulations étaient possibles, les valeurs obtenues de log K de Mn(II) et Sr(II) sont très différentes de celles de la littérature obtenues dans des conditions contrôlées. La nécessité d'un nouveau modèle conceptuel concernant plusieurs éléments traces et leur sorption est mis en avant, et ce, afin de mieux comprendre le devenir des contaminants dans les systèmes naturels.

INTRODUCTION

Carbonate minerals are widely present in natural environments, be they in a surface, subsurface or marine context (Reeder, 1983). Their high reactivity is also well established and implies several phenomena such as precipitation/dissolution and sorption/desorption, which control the availability and transport cycles of many chemical elements. A lot of studies have been carried into the surface behavior of calcite regarding divalent metallic cations to obtain the surface exchange properties of this mineral. At the macro scale, calcite powder equilibrated with water at various salinities is exposed to a given Me(II) concentration, and the evolution of the metal concentration in solution is measured along time or a pH path (Lakshtanov and Stipp, 2007; Tertre *et al.*, 2010; Zachara *et al.*, 1991, 1988). At the micro scale, spectroscopic, atomic force microscopy and synchrotron investigations are carried out to provide a better mechanistic representation of the processes happening at the calcite-liquid interface (Elzinga and Reeder, 2002; Freij *et al.*, 2005; Pokrovsky *et al.*, 2000; Stipp, 1999; Villegas-Jiménez *et al.*, 2009a, b). The data obtained from those experiments allowed the authors to constrain Surface Complexation Models (SCM) for several carbonate minerals, but uncertainties remain regarding the mechanistic description used in those models. For example, the two-site scheme based on the 1014 plan classically used for SCM reactions (Stipp and Hochella, 1991; Wright *et al.*, 2001) was discussed recently and a new one-site scheme finally proposed (Villegas-Jiménez *et al.*, 2009b). This new scheme represents much better the results of spectroscopic investigations and also allows a simplification of the numerical models used for SCM.

Still, those studies present surface properties of calcite regarding a maximum of two divalent metallic cations: Ca(II) from equilibration of solid calcite with the liquid phase, and another Me(II) cation added in solution. As the aim of sorption experiments is to get data to constrain models in the natural context, the study of the behavior of several Me(II) seems necessary. More specifically, the effect of the competitive sorption of major cations (naturally present in solution or released by dissolution processes) and trace elements (from the same possible sources) should be investigated. The most studied trace elements regarding sorption on calcite are divalent transition metals (Cd, Co, Mn, Ni, Pb, Zn) and earth-alkaline elements (Ba, Sr). A batch or a stirred flow-through reactor is filled with calcite powder and a water of variable salinity and pH, and a given amount of the trace element is inserted (Lakshtanov and Stipp, 2007; Martin-Garin *et al.*, 2003; Zachara *et al.*, 1991). All the

publications on this subject agree that the time dependant plots of Me(II) concentration present a two step behavior: a rapid uptake of the trace element (adsorption), and a second slower phase (coprecipitation, recrystallization).

In this study, the aim was to obtain sorption data analogous to what would happen in a natural surface context, but also to set up a methodology that could be applied to subsurface conditions. An example of a use for this methodology could be the storage of nuclear waste in deep subsurface layers, the behavior of a radionuclide in such a context and its possible long term fate in association with either the mineral or the liquid phase (Bruno *et al.*, 1998; Curti, 1999; Pérez del Villar *et al.*, 2002). A second example concerns the case of geological CO_2 storage, where the acidification of water due to CO_2 injection dissolves a part of the rock, which can lead to the mobilization of significant amounts of trace elements (Kharaka *et al.*, 2009; Little and Jackson, 2010; Pauwels *et al.*, 2007). To replicate such behaviors, no equilibration of the liquid phase with the natural carbonate is achieved, to reproduce the response of a carbonate system to a flux of water coming from the reservoir. The initial pH is used to reproduce the arrival of two solutions coming from the reservoir storage: water in equilibrium with the water-CO_2 system and the water-CO_2-calcite system. In both cases, the mobilization of TE (Mn(II) and Sr(II)) is studied in addition to that of Zn(II), to consider the multi-component aspect in the system. The impact of other factors such as salinity and initial Zn(II) concentration is also investigated. The results obtained in the experiments are then used as input data for simulations with PHREEQC (Parkhurst and Appelo, 1999) with several aims:

- to check that equilibrium is reached regarding calcite dissolution,
- to obtain surface complexation constants,
- to discuss those values in the light of the available literature.

1 MATERIALS AND METHODS

1.1 Samples Origin and Preparation

Two carbonates are considered in this study: the Lavoux carbonate and the St-Emilion carbonate. The first one is dated from the Callovian period (164.7-161.2 MY) and is produced in a carrier located at Lavoux, France. It comes from a 20 m thick oolithic white carbonate which presents fine grains cemented with calcite (Bourgueil and Gabilly, 1971). The St-Emilion carbonate is located in the upper Oligocene 1B layer (Stampian, 33.9-23.03 MY, 30 m thick), in the north of the Aquitaine basin, France (Cerepi, 1997). More information concerning the St-Emilion site and this carbonate are available in the articles concerning the CO_2-Vadose project (Loisy *et al.*, 2013). Previous to all analyses and experiments, the carbonates are crushed and sieved to recover the 10-100 μm fraction with an average grain diameter of 40 μm. The powders are then ultrasonically cleaned five times in pure ethanol over 10 min in order to eliminate the fraction inferior to 10 μm (the supernatant was removed and replaced until it remained clear). Each powder is then rinsed with ultrapure deionized water (18.2 MΩ cm^{-1}) for 5 min and dried for 12 hours at 80°C. The efficiency of this procedure is checked with Scanning Electron Microscopy (SEM) and a laser scattering particle size distribution analyzer.

1.2 Solid Characterization

1.2.1 Chemical Composition

The crystallographic phases (more than 1% weight) are evidenced by X-Ray Diffraction (XRD) with a *PANalytical* X'Pert Pro diffractometer using the $CoK\alpha_1$ radiation ($\lambda = 0.1789$ nm). Each sample is analyzed in reflection mode with a 50 kV tension and a 30 mA intensity. The diffraction pattern is acquired over the 2θ range from 2 to 80° in continuous mode with a step size equal to 0.0167°, a time/step equal to 200 s and a scan speed about 0.0106°/s. A Soller slit of 0.04 radian and a divergence slit of 1/4° are set up for the incident beam optics; while for the diffracted beam optics, a Soller slit of 0.04 radian, an anti-scatter slit of 5 mm and a Fe filter are used. This qualitative measure is completed with a quantitative Rock-Eval 6 analysis. In this device, 10 mg of each sample are submitted to combustion in a closed system at temperatures from 300°C to 650°C with a heating rate of 25°C/min in the presence of an inert gas (pyrolysis cycle), and in an open system under synthetic air flow at temperatures from 300°C to 850°C with a heating rate of 20°C/min (oxidation cycle). The CO and CO_2 produced by the decarbonation are measured as a function of the temperature for each cycle and allow us to distinguish organic carbon from mineral carbon, and even to determine the nature of the cations related to CO_3^{2-} groups (Behar *et al.*, 2001; Garcia *et al.*, 2010; Lafargue *et al.*, 1998). The mass balance obtained, coupled with the XRD analysis, allows the calculation of the weight percentage of each evidenced phase.

In order to analyze the TE content of the samples, each one is completely dissolved according to the procedure used by Le Pape *et al.* (2012). Half of the final solution obtained is diluted 10 times while the other half is diluted 100 times. Those two solutions are then analyzed with an ELAN 6100 (*Perkin-Elmer*) ICP-MS, calibrated from 0 to 100 μg/L for Mn, Zn and Sr (*Spex Certiprep*, Stanmore, UK). An external quality control is also analyzed to assess a 5% accuracy of the measured concentration.

1.2.2 Morphology and Petrophysics

The microscopic analyses of initial and reacted minerals are performed on a *Zeiss* EVO MA10 scanning electron microscope on Au coated samples. The sample morphology is imaged in classical SEM mode with a beam energy of 15 kV, the chemical contrast is monitored in backscattered electron mode with beam energy of 15 kV and the operating conditions for punctual analysis (EDS) are HT = 15 kV, I_{probe} = 700 pA, the dead time of detection being below 25%. The Specific Surface Area (SSA) of each powder is measured, after 12 hours of drying at 110°C, with an ASAP 2000 (*Micromeritics*) using the three point BET method with Kr as the adsorbent gas, as calcite often presents low values of SSA (below 1 m²/g). The estimated accuracy based on repeated measurements is below 10% for 1 g of carbonate.

1.3 Experimental Data

1.3.1 Apparatus and Analysis

The different sorption experiments are performed in 50 mL polypropylene beakers at $P_{CO_2} = 10^{-3.5}$ atm and consist of one gram of carbonate powder with 40 mL of one of the solutions (Tab. 1), thus 25 g/L of sorbent. The solid samples are dried at 90°C for ~ 30 min before each experiment to avoid over-estimation of the sample mass due to adsorbed water (Daval *et al.*, 2009). The initial pH is adjusted by addition of NaOH (0.01 M) or HCl (0.01 M). All the experiments are run at ambient temperature (~ 20°C), with an initial stirring. Four milliliters of solution are sampled after 24, 95, 196 and 363 hours of the experiment with the Lavoux carbonate and after 22.5, 88.5, 211 and 383 hours of the experiment with the St-Emilion carbonate. All these samplings are realized with polypropylene syringes, filtered through a 0.2 µm membrane, and immediately diluted (two times) in an acidified (0.2% HNO_3) solution for subsequent analysis. At the end of the experiments, 2 mL of solution is sampled for Ca(II) analysis and the solid phase is recovered by Büchner filtration using a 0.2 µm mesh size filter.

Before each sampling, the pH of the solution is measured with a *Mettler Toledo* SevenGo pro pH-meter calibrated with three NIST solutions (pH 4.01, pH 6.00 and pH 9.21) at 20°C. The trace element, Zn(II), Mn(II) and Sr(II), concentrations in solution are measured by ICP-AES (IRIS Advantage, *Thermo*), after an optimization of the injection and plasma conditions. An external calibration from 0 to 1 000 µg/L of each element (*Spex Certiprep*, Stanmore, UK) is done using NaCl 50 g/L solutions (*VWR*, GPR Rectapur 99%) as matrix matched solutions. Preliminary analyses were carried out in order to test the repeatability and the sensitivity of the instrument with the 50 g/L NaCl matrix. As for the ICP-MS analyses, an external quality control is also analyzed to assess a 5% accuracy of the measured concentration. The Ca(II) concentration at the end of the experiments is measured with a IonPac® CG12A Guard Column and CS12A Analytical Column (*Dionex*) after calibrations with both deionized and saline solutions. It is performed for an aqueous and for a saline solution (100 g/L) from 50 to 1 000 µmol/L of each element. Every ten samples analyzed, a blank and a control (200 µmol/L) are introduced to check that no drift occurs.

To complement the aqueous analyses, the reacted solid phases are studied with all the analytical methods presented in Section 1.2, but also by microprobe. To do so, reacted powders are prepared with epoxy resin in the shape of a pastille, then polished with heptane to obtain sections of grains and finally metalized with carbon. Those preparations are analyzed with a *JEOL* 8100 electron probe microanalyzer fitted with 5 wavelength dispersive spectrometers in order to investigate the zinc content of the reacted grains and more specifically the repartition profile of the zinc. To carry out this investigation, punctual analysis by steps of about 5 µm across the length of grains are realized, with a 25 kV acceleration voltage and a 240 nA beam current. Characteristic lines are measured with spectrometers: Si Kα on TAP, Ca Kβ on LiFH and Zn Kα on LiFH. C and O content are calculated by stoichiometry assuming Ca as $CaCO_3$, Si as SiO_2 and Zn as metal. The procedure developed by Armstrong (1988) is used for matrix correction. The position of background measurements is chosen at both sides of the peaks to avoid interferences, and subtraction is performed assuming a linear background. The counting time is 40 s on peaks and background, leading to a detection limit of 75 ppm for Zn. Standards are acquired just before measurement on albite for Si, on apatite for Ca and zinc sulfide for Zn.

1.3.2 Supplementary Calculations/Data Processing

The proportion of adsorbed zinc for each experiment is calculated with the formula:

$$\mathrm{Zn(II)}_{\mathrm{sorbed}} = \frac{\left([\mathrm{Zn(II)}]_i - [\mathrm{Zn(II)}]_f\right) \times 100}{[\mathrm{Zn(II)}]_i} \quad (1)$$

where $\mathrm{Zn(II)}_{\mathrm{sorbed}}$ is expressed in percent of the initial Zn(II) concentration, and $[\mathrm{Zn(II)}]_i$ and $[\mathrm{Zn(II)}]_f$ are the initial and final Zn(II) concentration in the solution in mol/L, respectively.

The calcite mass dissolved is calculated with the formula:

$$M_{diss} = \frac{[\mathrm{Ca(II)}]_f \times V_i}{M_{\mathrm{CaCO_3}}} \quad (2)$$

TABLE 1
Initial conditions of sorption experiments

Experiment ID	Carbonate	Salinity (g/L NaCl)	M_i, initial mass of powder (g)	$[Zn(II)]_i$ (mol/L)	pH_i	Equivalent equilibrium
1	Lavoux	/	1.0002	10^{-4}	4.12	Water CO_2 calcite
2	Lavoux	/	1.0001	10^{-5}	3.69	
3	Lavoux	/	1.0006	10^{-6}	3.53	
4	Lavoux	100	0.9996	10^{-4}	4.11	
5	Lavoux	100	1.0000	10^{-5}	3.51	
6	Lavoux	100	1.0008	10^{-6}	3.36	
7	Lavoux	/	0.9998	10^{-4}	2.97	Water CO_2
8	Lavoux	/	0.9998	10^{-5}	2.61	
9	Lavoux	/	1.0004	10^{-6}	2.54	
10	Lavoux	100	1.0005	10^{-4}	3.08	
11	Lavoux	100	1.0000	10^{-5}	3.00	
12	Lavoux	100	1.0009	10^{-6}	2.91	
13	St-Emilion	/	1.0003	10^{-4}	4.11	Water CO_2 calcite
14	St-Emilion	/	1.0005	10^{-5}	3.68	
15	St-Emilion	/	0.9997	10^{-6}	3.60	
16	St-Emilion	100	1.0004	10^{-4}	4.11	
17	St-Emilion	100	1.0001	10^{-5}	3.51	
18	St-Emilion	100	1.0001	10^{-6}	3.70	
19	St-Emilion	/	1.0001	10^{-4}	2.85	Water CO_2
20	St-Emilion	/	1.0003	10^{-5}	2.83	
21	St-Emilion	/	1.0000	10^{-6}	2.71	
22	St-Emilion	100	1.0001	10^{-4}	2.97	
23	St-Emilion	100	1.0000	10^{-5}	2.83	
24	St-Emilion	100	1.0003	10^{-6}	2.83	

where M_{diss} is the dissolved calcite mass in g, $[Ca(II)]_f$ is the Ca(II) concentration measured at the end of the experiment in mol/L, V_i is the initial volume used in the experiment in L and M_{CaCO_3} is the molar weight of calcium carbonate in g/mol. This calculation implies that the equilibrium of calcite dissolution is achieved within the first 25 hours of the experiments (before the first sampling). This hypothesis is considered valid as calcite is well known for its minute-scale dissolution (Villegas-Jiménez *et al.*, 2009a). From this calcite mass dissolved, the theoretical amount of TE released in solution is estimated considering an homogeneous repartition of the TE in the grains. To do so, the following equation is used:

$$n_{Me(II)} = \frac{[Ca(II)]_f \times V_i \times M_{CaCO_3} \times A_{TE}}{10^6 \times M_{TE}} \quad (3)$$

where $[Ca(II)]_f$ is the calcium concentration at the end of the experiment in mol/L, V_i is the volume of solution at the beginning of the experiment in L, M_{CaCO_3} is the molar weight of the calcium carbonate in g/mol, A_{TE} is the natural carbonate's content of TE (mg/kg) and M_{TE} is the molar weight of the TE considered in the calculation.

1.4 Simulations

The geochemical code PHREEQC (Parkhurst and Appelo, 2013) is used in order to simulate both dissolution and sorption processes under the experimental conditions described in Table 1. The following section presents the methodology used to carry out those simulations.

1.4.1 Database Selection

The question of the database is very important concerning simulations, especially when half of the experiments are performed in high salinity solutions (100 g/L of NaCl, *i.e.* 1.71 M). Indeed, the extended Debye-Hückel model used in PHREEQC for the calculation of the activity coefficient is considered valid for solutions with ionic strengths below 1 M (Parkhurst and Appelo, 1999), which is about half of the current salinity. Simulations were performed with both a Debye-Hückel and a Pitzer model (minteq.v4.dat and pitzer.dat databases respectively), and a maximum of 20% of the Ca(II) concentration underestimation was observed for simulations run with the classic model at this salinity (see Appendix). More precisely, this underestimation was comprised between 16% and 20% for basic initial conditions and around 10% for acid initial conditions. In the end, the lack of values for the elements studied in this paper forbade using Pitzer's database. The database minteq.v4.dat with the classic Debye-Hückel model for the calculation of the activity coefficient is thus used for all the subsequent simulations, despite its inadequacy for high salinity conditions. This is a recurrent issue for people working in high salinity systems, as stated in other studies (De Lucia *et al.*, 2012).

1.4.2 Equilibrium in the System

1.4.2.1 Calcite Dissolution Equilibrium

To ensure that our experiments match the equilibrium hypothesis, simulations are run using initial experimental conditions as input data: temperature, zinc concentration, pH, salinity, quantity of water, number of moles of calcite and partial CO_2 pressure. The initial pH is calculated as the quantity protons coming from the zinc solution and from the HCl or NaOH added to prepare the experimental aqueous and saline solutions: the results of those calculations are given in Table 1, as "pH_i". A maximum 10% difference is calculated between the measured pH in the remaining initial solutions and calculated initial pH values (data not shown).

1.4.2.2 Thermodynamic Precipitation of Secondary Phases

The selection of the database is also justified by the amount of data available concerning equilibrium of other mineral phases. Indeed, several chemical elements (Zn(II), Mn(II) and Sr(II)) at various concentrations are considered in this study and could lead to precipitation of other mineral phases. For example, in the phase diagram of the system $\{Zn - H_2O - CO_2\}$ the point corresponding to the conditions of this study belongs to the hydrozincite ($Zn_5(OH)_6(CO_3)_2$) predominance area (Preis and Gamsjäger, 2001). The possible precipitation of this phase is often discussed in the literature, especially for zinc concentrations above 10^{-5} M (Zachara *et al.*, 1991), thus its dissolution equilibrium value was taken from the database 'thermo.com.V8.R6.230' (Johnson *et al.*, 1992) and added to the database used in this study. The solubilities of phases related to Mn(II) and Sr(II) mineral species are numerous in the database, and as for hydrozincite, its saturation index is checked at the end of the simulations.

1.4.3 Surface Complexation Model (SCM)

The experimental results are used as an input dataset for surface complexation model simulations. The simulation of sorption is designed as a two-site SCM, according to the large literature available (Lakshtanov and Stipp, 2007; Martin-Garin *et al.*, 2003; Pokrovsky *et al.*, 2000; Stipp, 1999; Villegas-Jiménez *et al.*, 2009b). The equilibrium equations accounting for surface complexation in the context of the study are presented in Table 2 with the related log K values at 25°C and $I = 0$. The equilibrium constants concerning the three elements of interest in this study are initially taken to be equal to values from the literature: Glasner and Weiss (1980), Tsusue and Holland (1966) and Zachara *et al.* (1991). Two types of SCM simulation are run: in the first, only Zn(II) ions interact with the surface. For each experiment, the log K value for equation 07 (Tab. 2) is adjusted until the aqueous zinc concentration obtained and the final zinc concentration measured experimentally differs by less than 1%. In the second run, the whole system (Zn(II), Mn(II) and Sr(II)) is considered by adding the concentrations of the TE as an input data when a sorption calculation is possible. The fitting procedure is a bit more complex: the log K value for Zn(II) is fitted first, and then corrected as the log K values for Mn(II) and Sr(II) are also fitted. Several iterations of this procedure are necessary to obtain a difference lower than 1% between experimental and simulated concentrations for all elements.

2 RESULTS

2.1 Unreacted Samples

2.1.1 Mineral Phases, Carbon and TE

The XRD investigation of the natural carbonates (Fig. 1a) identified two main phases present in each carbonate by comparison to the reference diffractograms of those pure phases (Morris *et al.*, 1981; Swanson *et al.*, 1954).

TABLE 2

Surface complexation reactions relevant for the present system at 25°C and $I = 0$, used in PHREEQC. Data for reactions 01 to 06 from (Pokrovsky *et al.*, 2000); log K for reactions 07, 08 and 09 are determined from experimental results and presented in Table 5

	Reactions	Surface complexation equilibrium reactions	log $K°_{int}$ (25°C, $I = 0$)
Data from literature and thermodynamic databases	01	$CaOH^{\circ} - H^{+} = > > CaO^{-}$	−12
	02	$CaOH^{\circ} + H^{+} = > CaOH_2^{+}$	11.5
	03	$CaOH^{\circ} + CO_3^{2-} + 2H^{+} = > CaHCO_3^{\circ} + H_2O$	23.5
	04	$CaOH^{\circ} + CO_3^{2-} + H^{+} = > CaCO_3^{-} + H_2O$	17.1
	05	$CO_3H^{\circ} = > CO_3^{-} + H^{+}$	−5.1
	06	$CO_3H^{\circ} + Ca^{2+} = > CO_3Ca^{+} + H^{+}$	−1.7
Fit from experimental data	07	$CO_3Ca^{+} + Zn^{2+} = > CO_3Zn^{+} + Ca^{2+}$	
	08	$CO_3Ca^{+} + Sr^{2+} = > CO_3Sr^{+} + Ca^{2+}$	
	09	$CO_3Ca^{+} + Mn^{2+} = > CO_3Mn^{+} + Ca^{2+}$	

The presence of calcite is shown by the presence in both samples of the peak located at 34.3° (main calcite peak) and several others peaks (27, 42, 46, 51, 56 and 57°). For quartz, only the main peak (located at 31°) is detected clearly in the St-Emilion carbonate, while it is barely visible for the Lavoux carbonate. The results of the Rock-Eval 6 analyses are plotted in Figure 1b, and represent the quantity of CO_2 emitted during the pyrolysis cycle (dotted line) and during the oxidation cycle (full line). For both initial natural carbonates, the intensity of the peak obtained during the pyrolysis cycle is about 45 times less important than the peak obtained during the oxidation cycle. This information, combined with the temperature of the maximum CO_2 production, confirm that:

– no organic carbon (*i.e.* organic matter) is present in those samples, and
– that mineral carbon is contained by $CaCO_3$ (Lafargue *et al.*, 1998).

Those values allow the calculation of the initial proportion of $CaCO_3$ in the samples, according to Behar's methodology (Behar *et al.*, 2001). The compositions obtained are presented in Table 3, assuming that quartz is the only other phase present in the samples (a hypothesis which is confirmed by the SEM-EDXS analyses on initial carbonates, data not shown). The results of the ICP-MS analysis for TE are also given in Table 3 and complete the geochemical initial characterization of the samples. Both carbonates present a similar content of Zn and Sr but there is close to 10 times as much Mn in the St-Emilion carbonate than in the Lavoux carbonate.

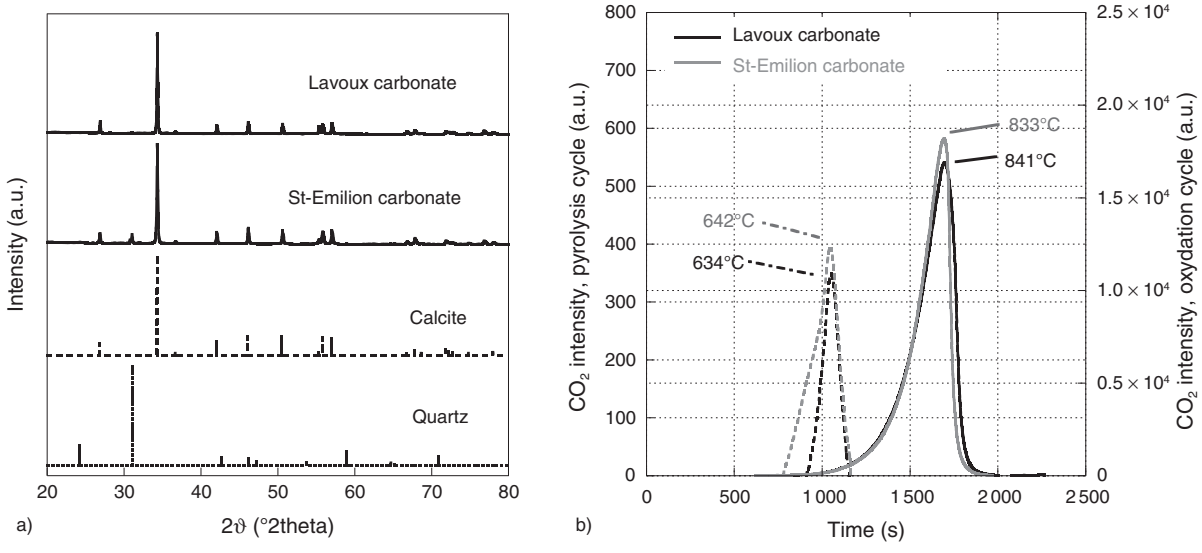

Figure 1

a) Plots of the Lavoux and the St-Emilion natural carbonates XRD analysis and those of pure calcite and quartz. Diffractograms are normalized with respect to their highest peak. b) Comparative Rock-Eval 6 analysis of the Lavoux and the St-Emilion carbonates. Dotted lines represent the pyrolysis cycle (intensity scale on the left axis) whereas full lines represent the oxidation cycle (intensity scale on the right axis).

2.2 Experimental Results

2.2.1 pH, Calcite Dissolution and TE Release

After about 200 hours of reaction the pH reaches a stable value in all the experiments: for pure water its mean value is 8.11, while it is 8.20 for brine experiments. The results for the final Ca(II) concentration (Tab. 4) show that salinity enhances dissolution by a factor of two for an initial basic pH, as seen in a paper from Coto *et al.* (2012), while it has no noticeable impact on dissolution when the initial pH is acid. The corresponding amount of calcite dissolved in each experiment is then calculated: this value ranges from 1.9 (experiment 14) to 8.4 mg (experiment 9); with a mean value of ~ 4 mg of calcite dissolved. This represents less than 1% of the initial solid phase present in the experiments, a value which is commonly used in the literature (Martin-Garin *et al.*, 2003; Tertre *et al.*, 2010; Villegas-Jiménez *et al.*, 2009b) to ensure that sorption is dominant regarding dissolution. In addition, the quantity of TE released in solution is calculated for each experiment. The released amount of Zn(II) is estimated to a concentration of 10^{-8} M, which is neglectible by comparison with the initial Zn(II) present in solution. Unfortunately, the results obtained for the maximum theoretical concentrations of Mn(II) and Sr(II) are in most cases lower than the experimental data. Thus, the sorption of those elements has to be approached differently, as discussed in the appropriate section.

2.2.2 Sorption

The behaviors of Zn(II), Mn(II) and Sr(II) are presented considering the evolution of their aqueous concentrations with respect to time (Fig. 2, 3).

2.2.2.1 pH Equivalent to Calcite-Water-CO_2 Partial Equilibrium in Geological Storage Conditions

Independently of the $[Zn(II)]_I$, of the salinity and of the natural carbonate (experiments 1-6;13-18, Tab. 1), a rapid decrease of [Zn(II)] occurs between 0 and 24 hours (Fig. 2a, b). This decrease is followed by either a stable [Zn(II)] value or a much slower sorption rate. This behavior is well-known in the literature (Zachara *et al.*, 1991), and is discussed in the appropriate section. The Zn(II) sorption calculations (Tab. 4) show that the presence of NaCl is the main control of the amount of Zn(II) sorbed, followed by the initial Zn(II) concentration.

In Figure 2c, the concentration of Mn(II) after 24 hours of reaction is the same (around 6×10^{-7} M), independent of the salinity and the initial Zn(II) concentration. Without NaCl, the Mn(II) concentration decreases more than in the presence of salt, and two different behaviors are evidenced at the end of the batch experiments. In brine systems, the end concentration of Mn(II) is approximately 2×10^{-7} M; while without salt it is ten times lower. In Figure 2d, the Mn(II) concentration is close to 7×10^{-6} for the first sample (24 hours of reactions), given the high uncertainty on the two lower points. The end concentration without salt is around 5×10^{-8} M and 5 times higher in brine. Independently of the natural carbonate considered, salinity clearly inhibits sorption of Mn(II). The behavior of Sr(II) released by the dissolution of the Lavoux carbonate is presented in Figure 2e. The first measures of Sr(II) concentration are higher in non-saline systems (between 1×10^{-6} and 3×10^{-6} M) than with NaCl (~ 6×10^{-7} M). In both cases, Sr(II) concentration decreases and there is evidence that the sorption of this element is enhanced by a factor 5 in the presence of NaCl. In Figure 2f, the Sr(II) concentration in pure water decreases from 8×10^{-6} to 8×10^{-5} M, divided by ten; while in the presence of salt, it decreases from $3\text{-}4\times10^{-6}$ to 1.6×10^{-7} M, divided by a factor close to twenty. Contrary to Mn(II), salinity enhances the sorption of Sr(II), independently of the natural carbonate considered.

To perform sorption calculations in the subsequent parts of this study, the higher concentration measured in an experiment is considered as an initial concentration. This is a consequence of the invalidity of the calculations relying on the hypothesis of homogeneous distribution of the TE in the powders (Sect. 2.2.1).

TABLE 3
Composition of the initial rock samples and the parameters necessary for the simulation of sorption

		Lavoux	St-Emilion
Composition	Calcite (%wt)	100 ± 2	96 ± 2
	Quartz (%wt)	0 ± 2	4 ± 2
	A_{Mn} (ppm)	33.4	282.8
	A_{Zn} (ppm)	29.0	16.6
	A_{Sr} (ppm)	160.6	180.9
	Initial SSA (m^2/g)	0.60	1.20
Sorption simulation parameters	Average reacted SSA (m^2/g)	0.53	1.10
	Density of surface sites ($moles/m^2$)	8.22×10^{-6}	8.22×10^{-6}
	Number of available surface complexation sites (moles)	4.357×10^{-6}	9.042×10^{-6}

2.2.2.2 pH Equivalent to Water-CO_2 Equilibrium in Geological Storage Conditions

A different trend is observed for zinc sorption with respect to time (Fig. 3a, b). The apparent sorption rate is much slower: it

TABLE 4

Results of calcite dissolution measurements, final Zn(II) concentrations and the related amount sorbed, initial and final concentrations for Mn(II) and Sr(II) estimated and measured in sorption experiments along with the estimated amount of TE sorbed

Experiment ID	Final pH	$[Ca(II)]_{final}$ measured (μmol/L)	Dissolved calcite, calculated (mg)	$[Zn(II)]_{final}$ (mol/L)	$Zn(II)_{sorbed}$ (%)	$[Mn(II)]_i$ (mol/L)	$[Mn(II)]_{final}$ (mol/L)	$Mn(II)_{sorbed}$ (%)	$[Sr(II)]_i$ (mol/L)	$[Sr(II)]_{final}$ (mol/L)	$Sr(II)_{sorbed}$ (%)
1	7.89	571.7	2.3	1.1955×10^{-5}	88.0	5.95×10^{-7}	2.9×10^{-8}	95.20	8.48×10^{-7}	5.25×10^{-7}	38.07
2	8.07	502.4	2.0	1.058×10^{-6}	89.4	7.49×10^{-7}	1.7×10^{-8}	97.67	1.001×10^{-6}	4.11×10^{-7}	58.92
3	8.13	553.9	2.2	1.23×10^{-7}	87.7	6.80×10^{-7}	1.9×10^{-8}	97.18	2.758×10^{-6}	4.76×10^{-7}	82.76
4	8.17	1154.0	4.6	1.8203×10^{-5}	81.8	5.21×10^{-7}	1.73×10^{-7}	66.82	5.47×10^{-7}	1.08×10^{-7}	80.19
5	8.24	1093.8	4.4	6.45×10^{-7}	93.6	4.98×10^{-7}	1.86×10^{-7}	62.62	6.21×10^{-7}	1.17×10^{-7}	81.21
6	8.21	1060.7	4.2	3.1×10^{-8}	96.9	/	2.52×10^{-7}	/	/	1.58×10^{-7}	/
7	8.03	1083.3	4.3	1.2522×10^{-5}	87.5	8.6×10^{-8}	1.6×10^{-8}	82.00	/	7.23×10^{-7}	/
8	8.12	1815.7	7.3	4.48×10^{-7}	95.5	8.2×10^{-8}	1.0×10^{-8}	87.57	/	1.087×10^{-6}	/
9	8.07	2101.3	8.4	1.52×10^{-7}	84.7	2.23×10^{-7}	4.0×10^{-8}	81.98	2.053×10^{-6}	1.308×10^{-6}	36.21
10	8.16	1263.8	5.1	2.1040×10^{-5}	78.9	/	1.91×10^{-7}	/	/	1.20×10^{-7}	/
11	8.25	1154.8	4.6	7.35×10^{-7}	92.7	/	1.72×10^{-7}	/	/	1.08×10^{-7}	/
12	8.24	1138.2	4.6	3.8×10^{-8}	96.1	/	2.20×10^{-7}	/	/	1.38×10^{-7}	/
13	7.96	539.2	2.2	1.0078×10^{-5}	89.9	9.4×10^{-8}	6.6×10^{-8}	29.95	/	7.20×10^{-7}	/
14	8.09	462.7	1.9	4.55×10^{-7}	95.4	1.0401×10^{-5}	5.3×10^{-8}	99.49	7.448×10^{-6}	7.61×10^{-7}	89.79
15	8.14	516.2	2.1	1.14×10^{-7}	88.6	7.682×10^{-6}	4.8×10^{-8}	99.38	7.921×10^{-6}	8.53×10^{-7}	89.23
16	8.15	1267.7	5.1	2.9616×10^{-5}	70.4	7.579×10^{-6}	2.51×10^{-7}	96.69	3.502×10^{-6}	1.57×10^{-7}	95.51
17	8.24	1312.3	5.3	9.76×10^{-7}	90.2	5.551×10^{-6}	2.83×10^{-7}	94.90	3.709×10^{-6}	1.77×10^{-7}	95.22
18	8.21	1599.0	6.4	5.4×10^{-8}	94.5	/	2.74×10^{-7}	/	/	1.72×10^{-7}	/
19	8.18	1121.6	4.5	1.1518×10^{-5}	88.5	1.34×10^{-7}	1.23×10^{-7}	8.20	/	1.08×10^{-6}	/
20	8.30	1161.1	4.6	7.35×10^{-7}	92.6	1.38×10^{-7}	1.09×10^{-7}	21.08	/	1.236×10^{-6}	/
21	8.32	1414.7	5.7	1.35×10^{-7}	86.5	3.30×10^{-7}	1.49×10^{-7}	54.74	2.240×10^{-6}	1.420×10^{-6}	36.60
22	8.18	1251.5	5.0	3.1825×10^{-5}	68.2	/	2.74×10^{-7}	/	2.47×10^{-7}	1.72×10^{-7}	30.39
23	8.14	1198.3	4.8	1.298×10^{-6}	87.0	/	2.70×10^{-7}	/	2.89×10^{-7}	1.69×10^{-7}	41.41
24	8.17	1168.9	4.7	9.6×10^{-8}	90.4	4.62×10^{-7}	2.86×10^{-7}	38.10	/	1.79×10^{-7}	/

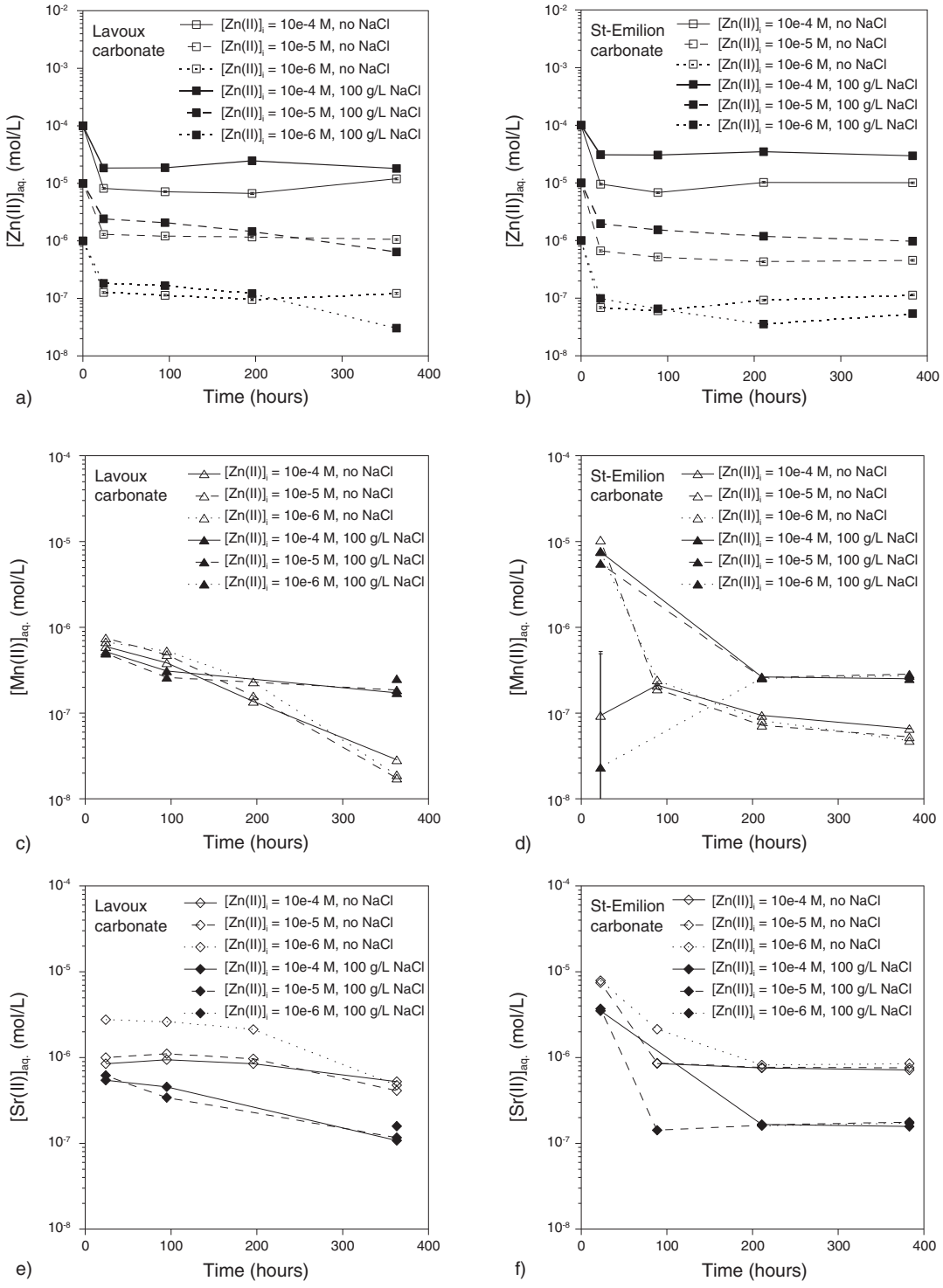

Figure 2

Results of sorption experiments considering an initial water-CO_2-calcite equilibrium. a,b) Zinc concentration evolution as a function of time for experiments performed with the Lavoux and the St-Emilion carbonate in aqueous (empty symbols) and saline solution (black symbols): $[Zn(II)]_i$ equal to 10^{-4} M (full line), 10^{-5} M (dotted line), 10^{-6} M (dashed line). c,d) Evolution with time of [Mn(II)]. The same code as for plots a) and b) is used. When not visible, error bars are comprised within the symbol size. e,f) Evolution with time of [Sr(II)]. The same code as for plots a) and b) is used. When not visible, error bars are comprised within the symbol size.

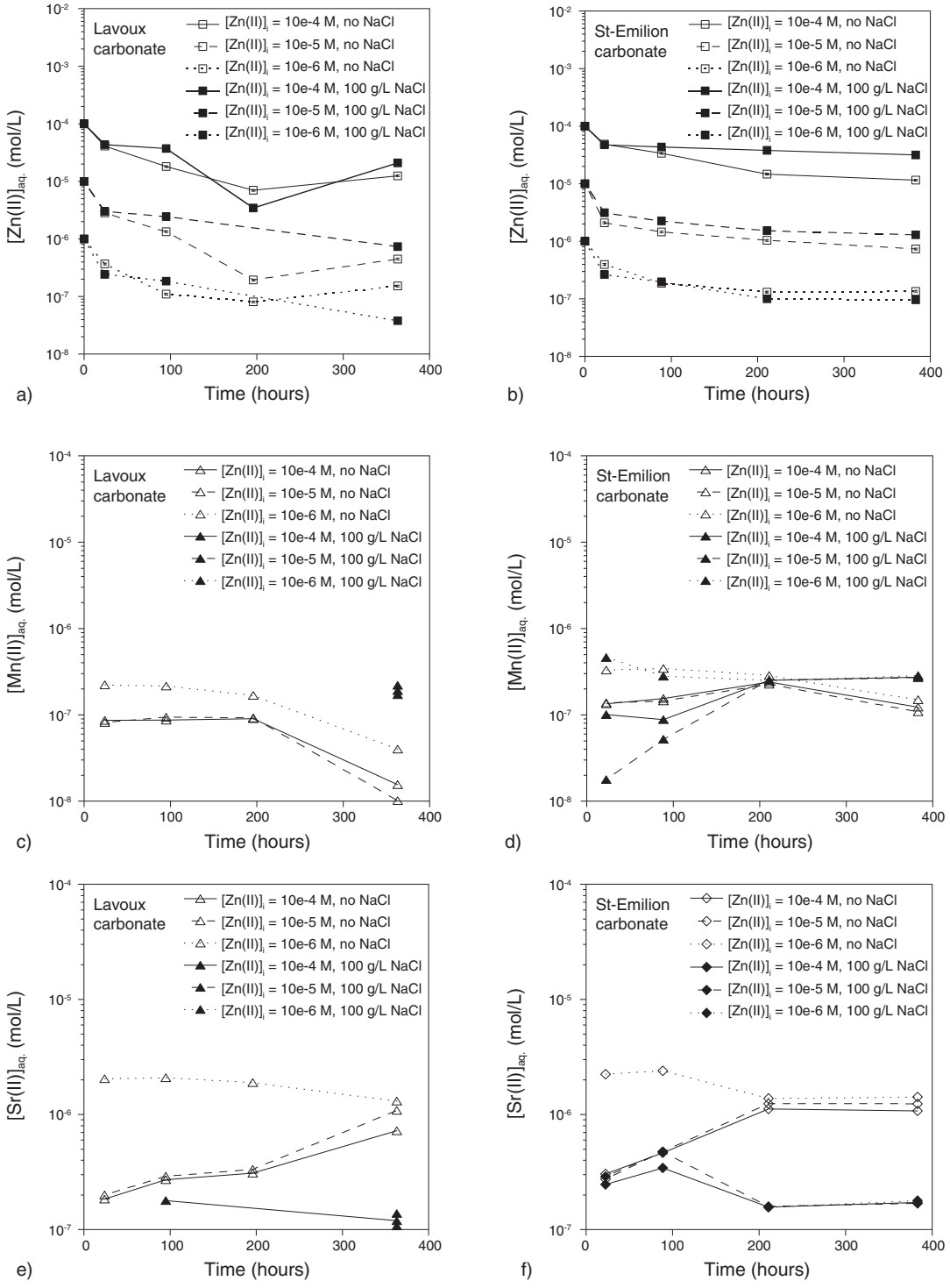

Figure 3

Results of sorption experiments considering an initial water-CO_2 equilibrium . a,b) Zinc concentration evolution as a function of time for experiments performed with the Lavoux and the St-Emilion carbonate in aqueous (empty symbols) and saline solution (full black symbols): $[Zn(II)]_i$ equal to 10^{-4} M (full line), 10^{-5} M (dotted line), 10^{-6} M (dashed line). c,d) Evolution with time of [Mn(II)]. The same code as for plots a) and b) is used. When not visible, error bars are comprised within the symbol size. e,f) Evolution with time of [Sr(II)]. The same code as for plots a) and b) is used. When not visible, error bars are comprised within the symbol size.

takes about 200 hours to get to the concentration corresponding to 24 hours of reaction in the condition previously investigated (about 8 times as much time). Though, if we consider the zinc concentration values at the end (~ 380 hours) of the experiments, the values are nearly the same. Translated in terms of zinc sorbed (experiments 7-12 and 19-24, Tab. 4), a slight reduction (between 1% and 3%) of that quantity is observed, except for experiment 8, which shows a 7% higher zinc sorption, by comparison with experiment 2. Not taking into account this value, the same conclusion as for basic experiments can be stated: in pure water the initial Zn(II) concentration does not impact the amount of zinc sorbed, whereas in brine the amount of zinc sorbed increases when $[Zn(II)]_i$ decreases. The measured aqueous concentrations of Mn(II) and Sr(II) (Fig. 3c-f) are also higher than the maximum theoretical concentration, which confirms that the hypothesis of homogeneous repartition of TE in the sample is not proper, or that the TE content of initial samples was underestimated. Again, the same behavior is observed for both carbonates: there is less Mn(II) sorbed in high salinity experiments (7-12 and 19-24, Tab. 4), and the amount of Sr(II) sorbed is reduced by the salinity. This shows that initial pH only impacts the kinetics of the sorption phenomenon (factor 8 in time) for zinc. Though, the stronger dissolution that occurs in those conditions seems to impact the sorption kinetics of TE released in the system: in many of the experiments their concentrations present far fewer variations than in the basic conditions, and can even increase continuously (experiments 7, 8, 9, 19, 20, 23). The final concentrations of TE confirm that salinity is the major parameter controlling the amount of sorbed element.

2.2.3 Newly-Formed Phases and Surface Changes

Despite a careful study of the reacted samples with all the techniques used for initial characterization (Sect. 1.2), the presence of newly formed solid phases could not be evidenced, except locally with the presence of NaCl crystals in high salinity experiments (data not shown), which are not relevant in the present study. Enrichment in zinc on the periphery of the grains could only be evidenced after microprobe analysis, around 150 ppm for the Lavoux carbonate, and up to 700 ppm for the St-Emilion carbonate, as clearly shown in Figure 4. The SSA measurements of the reacted powders showed a decrease of 0.07 and 0.1 m^2/g for the Lavoux and the St-Emilion carbonate powder respectively by comparison with the non-reacted measurements.

2.3 Modeling Results

2.3.1 Simulation of Calcite Dissolution

The experimental values are then compared to the simulated concentrations obtained with PHREEQC (Tab. 5).

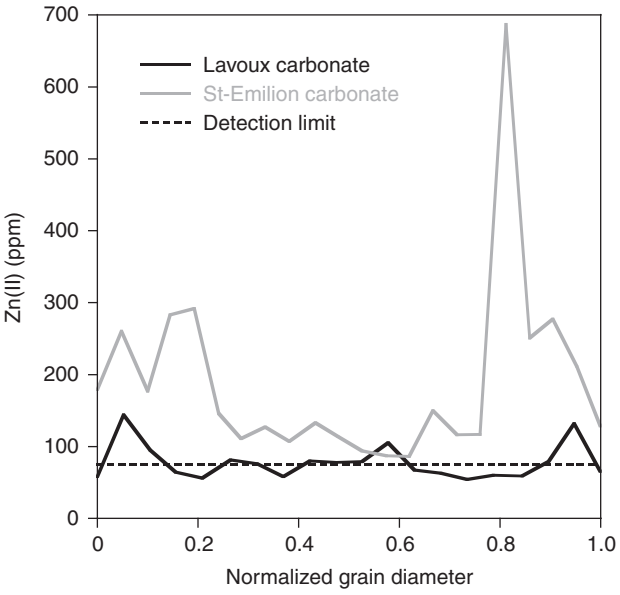

Figure 4

Microprobe analyses of reacted Lavoux and St-Emilion powder. Each profile represents the mean zinc content (ppm) of the cross-sections for 15 grains, in function of the grain radius normalized to 1. The dotted line represents the detection limit (75 ppm).

The final pH values obtained by simulation present a good match with the experimental measures, with a maximum difference of 5%. Concerning the concentration of Ca(II), the experiments in aqueous solution match well with the simulated data (only 1 value with over 20% difference between result and simulation); but as expected, due to the non adequacy of the database in high salinity solutions, dissolution is overestimated in simulations (up to 45% in terms of concentration).

2.3.2 Sorption Modeling Results

2.3.2.1 Zn(II) as the Only Metal Considered

The result of the fitting procedure for each experiment is given in Table 5 under the form of a log K value. All the log K values obtained are between 1.7 and 4.62, and can be specified according to the carbonate considered and to the salinity of the aqueous phase. The initial zinc concentration seems to control the log K value in non saline experiments: log K decreases when $[Zn(II)]_i$ decreases (experiments 1-3, 7-8 and 13-15). The absence of impact from the initial pH of the solution is observed again in the simulations: this leads the Lavoux carbonate to record log K = 2.56 +/– 0.52 in pure water and log K = 4.50 +/– 0.14 in brine; and for the St-Emilion

TABLE 5
PHREEQC simulation results of [Ca(II)] for calcite-solution-CO_2 equilibrium and log K values obtained for Zn(II) sole sorption, and multiple Zn(II), Mn(II) and Sr(II) sorption

			Zn(II) sorption	Zn(II), Mn(II) and Sr(II) sorption		
Experiment ID	$[Ca(II)]_{final}$ simulated (µmol/L)	Error (%)	log K_{Zn}	log K_{Zn}	log K_{Mn}	log K_{Sr}
1	560.5	1.99	3.05	3.08	3.35	1.84
2	606.6	−17.17	2.09	2.10	2.63	1.16
3	640.3	−13.49	1.99	2.00	2.53	1.67
4	1440.0	−19.86	4.58	4.60	4.93	2.69
5	1541.0	−29.02	4.32	4.32	4.06	1.93
6	1599.0	−33.66	4.62	/	/	/
7	958.2	13.05	3.17	3.18	2.89	/
8	1602.0	13.34	2.83	2.83	2.27	/
9	1847.0	13.77	2.24	2.25	2.09	1.18
10	1785.0	−29.19	4.52	/	/	/
11	1867.0	−38.15	4.33	/	/	/
12	1983.0	−42.60	4.61	/	/	/
13	561.2	−3.92	2.05	2.05	0.57	/
14	608.3	−23.94	2.15	2.20	3.01	1.65
15	623.9	−17.26	1.7	1.74	2.89	1.60
16	1440.0	−11.96	3.36	3.41	5.18	2.49
17	1541.0	−14.84	3.78	3.80	4.78	2.27
18	1495.0	6.96	4.01	/	/	/
19	1110.0	1.04	2.07	2.07	0.06	/
20	1140.0	1.85	2.13	2.13	0.35	/
21	1360.0	4.02	1.87	1.88	1.07	0.73
22	1903.0	−34.24	3.42	3.42	/	0.86
23	2129.0	−43.72	3.77	3.76	/	0.92
24	2111.0	−44.63	3.89	3.89	3.39	/

carbonate to log K = 1.99 +/− 0.17 in pure water and log K = 3.70 +/− 0.26 in brine. Whatever the carbonate considered, the log K value is higher in high salinity conditions.

2.3.2.2 Zn(II), Mn(II) and Sr(II) Considered

As for the simulation considering only zinc sorption, the results are given as log K values in Table 5. Firstly, the log K values for zinc sorption are slightly impacted when the sorption of several different species is considered: indeed the variations of those values are below 0.05 units whatever the experiment considered. Regarding log K obtained for Mn(II) and Sr(II), the variability of the behaviors observed in the experiments did not allow the authors to simulate all experiments. Especially in high salinity conditions, the first concentration measured (after ~24 hours) was often below the final concentration, preventing analysis of the data as a classic sorption phenomenon. Nevertheless, some trends

are clearly visible. First the relative importance of the log K values in experiments 1, 2, 3, 4, 14, 15, 16, and 17 (initial pH basic independent of the carbonate considered) is the same: $\log K_{Mn} > \log K_{Zn} > \log K_{Sr}$. When considering initial pH impact, the values obtained indicate that the log K values are lower when the initial pH is about 3, whether Mn(II) or Sr(II) are considered.

3 DISCUSSION

3.1 Equilibrium of the Dissolution/Precipitation Processes

The values obtained for equilibrium Ca(II) concentration in the simulations and the experiments (comparison in Tab. 5) are in good accordance for experiments in aqueous solution (only 1 value showed over 20% of difference between the result and simulation, experiment 14); but in high salinity solutions, the difference between experiment and simulation increases (between 12% and 45%). To explain those higher differences for high salinity, the main argument is the impact of the database used and especially of the classic Debye-Hückel model. Indeed, as presented in Section 1.3.1.1, a difference of up to 20% is introduced if we consider the Pitzer database as the reference (see Appendix). This variability can also be due to the interaction of calcite with solute species: Martin-Garin *et al.* (2003) evidenced that cadmium impacts the reactivity of the calcite crystal surface, as showed in previous studies (Dove and Hochella, 1993; Fenter *et al.*, 2000; Hillner *et al.*, 1992; Reeder, 1996). Also, some experiments present a Ca(II) concentration higher than the maximum value of the calibration range, which can lead to a drift in the measured value. Finally, the mean pH values obtained, 8.17 in pure water and 8.11 in brine, confirm the equilibrium hypothesis in the system, with only a few percent difference with the simulated value (8.27). Concerning the possible precipitation of newly formed phases, only hydrozincite presents, for some simulations, a positive Saturation Index (SI). This point is discussed specially for initial zinc concentrations above 10^{-5} M (Zachara *et al.*, 1991) and corresponds effectively to the predominance area of hydrozincite in the phase diagram of the system $\{Zn - H_2O - CO_2\}$ corresponding to the present conditions (Preis and Gamsjäger, 2001). Even though no hydrozincite presence was evidenced by all the techniques used in this study, thin deposits (~10 nm) could certainly have been distinguished with an atomic force microscope, as showed by Freij (Freij *et al.*, 2005). The solubility of phases related to Mn(II) and Sr(II) mineral species are numerous in the database used, and as for hydrozincite, their SI at the end of the simulations is sometimes slightly positive but again, it was never related to the observation of any newly formed phase. These discussions concerning dissolution, precipitation and equilibrium in the system ensure the validity of the major contribution of sorption in the interpretation of the results.

3.2 Sorption of Zn(II), Mn(II) and Sr(II)

The trends observed in Zn(II) concentration in the experiments are in good accordance with those observed in many studies (Freij *et al.*, 2005; Tertre *et al.*, 2010; Zachara *et al.*, 1988), as are the amounts of Zn(II) sorbed: whatever the initial conditions of the experiments the strong zinc retention by calcite is evidenced. But another aspect is emphasized here: the role of high salinity on the amount of zinc sorbed. Indeed, the 1.71 Meq ionic strength used in this study is much higher than in Zachara's experiments (maximum 0.03 M) and implies different amounts of Zn(II) sorbed, depending on the natural carbonate used and the initial concentration of Zn(II). This salinity impact could be due to the thickness of the diffuse double layer κ^{-1}, defined by $\kappa^{-1} \sim 3.09/(I^{1/2})$ where I is the ionic strength in mol/dm^3 in the Debye-Hückel theory (Appelo and Postma, 1993). From about 75 Å in pure water conditions, this thickness is reduced to ~2 Å in 100 g/L NaCl conditions, but such dimensions count only for a very small amount of the porous medium considered here. More probably, the surface speciation of calcite in such high salinities is not the same as in lower salinities, where it is much better understood and constrained (Pokrovsky *et al.*, 2000; Villegas-Jiménez *et al.*, 2009a). Despite this lack of knowledge regarding the surface speciation for all experimental conditions, the log K values obtained by simulation for zinc are in agreement with the values obtained by Zachara (Zachara *et al.*, 1988, 1991), even though they present a larger range due to the wider experimental conditions investigated. A supplementary point to discuss regarding those discrepancies is the log K dependence on standard states for activities of surface sites and species, as showed by Sverjensky (2003). The sorbent used (*i.e.* the natural carbonate), the number of surface sites, its SSA and the salinity of the solution strongly impact the log K values obtained. When the three elements are considered for sorption, we have showed (Fig. 2, 3) that an initial acid pH controls the appearance in solution of the TE by a slow increase of their concentration as the system tends towards a balance between the release of species in solution and the adsorption of these same released species. To the best of our knowledge, no such observation is mentioned in the literature, either because people who studied sorption did it in strictly controlled conditions with pre-equilibrated solutions (with regard to calcite SI) or because they were studying the sorption of one element on a specific sorbent. Despite the impossibility of interpreting all the data obtained as sorption data, log K values for Mn(II) and Sr(II) could be estimated. Those values are very different from those

presented in the literature, where sorption of those elements regarding calcite is studied. Concerning manganese, the values reported lie between 0.6 and 1.39 (Lorens, 1981; Pingitore *et al.*, 1988; Zachara *et al.*, 1991). For strontium, the values of the literature are all negative, lying between −2.04 and −0.52 (Mucci, 1986; Pingitore and Eastman, 1986, 1984; Zachara *et al.*, 1991). These discrepancies indicate that the values obtained in the studies regarding mono-element sorption added in solution are not relevant when multiple elements are considered, and are even less so when some of those elements are not initially in solution but released by the dissolution of the sorbent. Despite their mutual coherence, the log K values obtained are good in the sense that they match well the experimental data and indicate a scaling of sorption regarding initial pH and salinity. The kinetic processes controlling combined calcite dissolution and zinc sorption coupled with TE release and re-sorption are yet to be put in equations to constrain rigorously those phenomena, either in pure water or under high salinity conditions. It is all the more clearly evidenced when considering the experiments with an initial pH close to 3: only half of the data allowed a sorptive interpretation of the experiments.

3.3 Implications in Case of CO_2 Leakage Up to a Shallow Aquifer

The impact of a leakage is still one of the key issues connected with CO_2 geological storage as a remedy to carbon concentration increase in the atmosphere (IPCC, 2005). Uncertainties concerning the displacement of the CO_2 plume and fluids from the underground storage formation extend also to uncertainties concerning the species that could be released by the reactivity induced by the CO_2 or acid fluid influx. Indeed, it was clearly evidenced by field studies (Kharaka *et al.*, 2006) that the concentration of iron in solution was very sensitive to CO_2 injection, for example. Though, in such field studies, it is not possible to calculate the quantity of iron that stays in the liquid phase after being transported in the porous media across tens of meters. Another study, from Viswanathan *et al.* (2012), showed that the fate of arsenic in an aquifer subjected to natural CO_2 flux is a very challenging field in which to study this kind of reactive-transport with field scale data and laboratory experiments. They explain the immediate increase in As following CO_2 injection observed in their experiments by either the dissolution of calcite or As desorption from oxides and/or clays. It is coherent with the process that occurs in the experiments presented in this paper: the Mn(II) and Sr(II) concentrations increase from nought to a given concentration, depending on the quantity of carbonate dissolved and on the initial TE content in the natural carbonate. In particular, the equilibrium concentration of As that they measure and simulate after 25 days of experiments is not zero, which means that even if this concentration drops by a factor of 10 in this time lapse, there is still As available in solution. In this paper, the amount of zinc still available after reaching the equilibrium corresponds well to the values from the literature, with between 70% and 97% of zinc concentration decrease, but no such statement can be made concerning TE. Mn(II) and Sr(II) seem to be captured well by the solid when the initial pH is close to 4.7, but this is much less the case with an initial pH of 3. The salinity is also a major parameter, as we showed variations of up to 10% of the sorption of Mn(II) and Sr(II) according to this parameter. Knowing that in such experiments, the sorption capacity is enhanced (higher SSA, and no transport phenomenon) regarding natural processes, this shows clearly that the amount of such elements available in solution will imply higher values.

At the same time, in a natural system, other mineralogical phases are present, such as clay minerals that show very interesting sorption properties. Viswanathan *et al.* (2012) discuss the impact of the dissolution of clay surfaces and of the precipitation of small volume fractions of kaolinite that modify the number of sorption sites in their simulations, along with the strong impact of pH on sorption. Though, the observations on rock samples taken from various aquifers in Texas and the Gulf Coast region by Smyth *et al.* (2009) are different from the experimental results of this article. Their "Type I" class of elements that contains Zn, Mn and Sr corresponds to elements that stay in solution with no sorption. In the conditions of this study, those elements should be contained by the "Type II" class as their concentration increases rapidly and then decreases over time. The results presented here imply that the differentiation between sorbed and non-sorbed elements is certainly related to the sorbent used, and the affinity between the elements considered and this sorbent. The "scavenging" effect considered shows that in a natural carbonate context, those trace elements are relevant and behave in accordance with the sorbent used, as evidenced at natural analogue sites (Aiuppa *et al.*, 2005).

CONCLUSIONS

The sorption experiments presented in this paper evidence the impact of different factors such as initial pH, initial Zn(II) concentration and salinity of the liquid phase on the dissolution/precipitation and sorption phenomena. A combination of multiple experimental techniques allowed us to obtain data which we then used to run simulations with the geochemical code PHREEQC. The results obtained both experimentally and by simulations intend to prove that the behavior of TE in such systems remains to be more deeply investigated. Indeed some behaviors could not be modeled with the classical methods, including for example the

continuous release of Mn(II) and Sr(II) observed in experiments with an initial pH of about 3.

For all experiments, the equilibrium of the main kinetic phenomenon (fast Zn(II) uptake) was reached within 200 hours maximum, with either the end of sorption or a lower rate phenomenon occurring then. This sorption could neither be evidenced by SEM-EDX or XRD but it was possible to show an enrichment of the surface of the grains using the microprobe technique. Even though the dissolution was considered negligible (less than 1% of the initial powder mass was dissolved), the mobilization of trace elements was investigated. Mn(II) and Sr(II) concentrations were measured and their behavior regarding sorption established. The low amount of calcite dissolved implied strong variations in the composition of the solid-liquid interface. Concerning TE, not only the behaviors, but the equilibrium values observed were very dependent on the initial pH, showing that the sole sorption perspective is not adapted to consider the behavior of the gas-water-rock-TE assemblage. The concentration of the major element Ca(II) is constrained by calcite equilibrium, as is already well known, but there are two main factors controlling the evolution of elements in the system:

– the initial pH,
– the salinity of the water,

with a slight influence of initial Zn(II) concentration in brine. The simulations carried out with PHREEQC demonstrate that sorption of a relatively concentrated element (Zn(II) here) is well constrained by a simple log *K* value with the two site SCM scheme (Davis and Kent, 1990) used along with the equilibrium constants from the literature (Pokrovsky *et al.*, 2000; Villegas-Jiménez *et al.*, 2009b). However, these simulations remain dependent on the salinity and on the specific petrophysical and morphological properties of the natural carbonate (Sverjensky, 2003). The impossibility of carrying out several simulations showed that mathematical representation used is not relevant when one wants to consider the evolution of the TE released from the bulk solid in a natural carbonate system following dissolution, *i.e.* with an initial pH acid. In addition, the validity of the database used in high salinity conditions remains disputable, but no other possibility is currently available when one is interested in TE behavior.

In the context of a leakage from a CO_2 storage site into an aquifer closer to the surface, the potential consequences for water quality are clear: the strong reactivity of carbonate minerals, widely present on the surface of Earth (Reeder, 1983), could imply the release in solution of non-negligible amounts of potentially hazardous elements. The scavenging effect is thus a major center of interest in better understanding both the incorporation of TE in rocks and their mobility along the different geological reservoirs where gas-water-rock interactions occur.

These are the potential consequences for the hydrogeochemistry of subsurface water reservoirs, but a complementary study was also carried out to consider the scavenging effect under CO_2 geological storage conditions. Those conditions correspond indeed to a minimum of ~ 73 atm and 31°C, where the supercritical CO_2 injected in an aquifer is progressively dissolved and trapped in the reservoir formation, and imply many more dissolution reactions than in atmospheric conditions. Therefore, along with integrity studies and risk assessment investigations, the fate of TE mobilized in such conditions remains to be investigated in terms of the quantity of elements that will be definitively released in the aqueous phase and their competitive behavior regarding adsorption (Auffray *et al.*, 2016), and appropriate mathematical tools have yet to be built to simulate their migration along other natural compartments.

ACKNOWLEDGMENTS

B. Auffray is grateful to Frédéric Neyret-Martinez and Nathalie Texier for their presence and advice during the ICP-AES analyses campaign, to Anne-Sophie Gay and Yannick Blouet for their help concerning the microprobe analyses and to Véronique Bardin for their availability during the liquid chromatography analyses. The authors also thank the three anonymous reviewers who helped to substantially enlighten this article. This paper is part of the PhD Thesis of B. Auffray, funded by *IFP Energies nouvelles.*

REFERENCES

Aiuppa A., Federico C., Allard P., Gurrieri S., Valenza M. (2005) Trace metal modeling of groundwater-gas-rock interactions in a volcanic aquifer: Mount Vesuvius, Southern Italy, *Chemical Geology* **216**, 289-311.

Appelo C.A.J., Postma D. (1993) *Geochemistry, groundwater and pollution*, A.A. Balkema (ed.), Brookfield, VT.

Armstrong J.T. (1988) *Quantitative analysis of silicate and oxide materials: Comparison of Monte Carlo, ZAF, and Φ(ρz) procedures, Microbeam Analysis*, San Francisco Press.

Auffray B., Garcia B., Lienemann C.-P., Sorbier L., Cerepi A. (2016) Zn(II), Mn(II) and Sr(II) behavior in natural carbonate reservoir system. Part II : impact of geological CO_2 storage conditions, submitted to *Oil & Gas Science and Technology.*

Behar F., Beaumont V., Penteado H.L.D.B. (2001) Rock-Eval 6 Technology: Performances and Developments, *Revue de l'Institut Français du Pétrole* **56**, 111-134.

Bourgueil B., Gabilly J. (1971) *Carte géologique de la France n° 590 à 1/50 000*, Chauvigny.

Bruno J., Duro L., de Pablo J., Casas I., Ayora C., Delgado J., Gimeno M.J., Peña J., Linklater C., Pérez del Villar L., Gomez P. (1998) Estimation of the concentrations of trace metals in natural systems: The application of codissolution and coprecipitation

approaches to El Berrocal (Spain) and Poços de Caldas (Brazil), *Chemical Geology* **151**, 277-291.

Cerepi A. (1997) Milieux poreux matriciel, fractures et teneur en eau d'un calcaire en zone de diagenèse météorique : Calcaire à astéries "Pierre de Bordeaux", Oligocène (Bordeaux, France), *Ph.D. Thesis*.

Coto B., Martos C., Peña J.L., Rodríguez R., Pastor G. (2012) Fluid Phase Equilibria Effects in the solubility of $CaCO_3$: Experimental study and model description, *Fluid Phase Equilibria* **324**, 1-7.

Curti E. (1999) Coprecipitation of radionuclides with calcite: estimation of partition coefficients based on a review of laboratory investigations and geochemical data, *Applied Geochemistry* **14**, 433-445.

Daval D., Martinez I., Corvisier J., Findling N., Goffé B., Guyot F. (2009) Carbonation of Ca-bearing silicates, the case of wollastonite: Experimental investigations and kinetic modeling, *Chemical Geology* **265**, 63-78.

Davis J.A., Kent D.B. (1990) Surface Complexation Modeling in Aqueous Geochemistry, *Reviews in Mineralogy and Geochemistry* **23**.

De Lucia M., Bauer S., Beyer C., Kühn M., Nowak T., Pudlo D., Reitenbach V., Stadler S. (2012) Modelling CO_2-induced fluid-rock interactions in the Altensalzwedel gas reservoir. Part I: from experimental data to a reference geochemical model, *Environmental Earth Sciences* **67**, 563-572.

Dove P.M., Hochella Jr M.F. (1993) Calcite precipitation mechanisms and inhibition by orthophosphate: *In situ* observations by Scanning Force Microscopy, *Geochimica et Cosmochimica Acta* **57**, 705-714.

Elzinga E.J., Reeder R.J. (2002) X-ray absorption spectroscopy study of Cu^{2+} and Zn^{2+} adsorption complexes at the calcite surface: Implications for site-specific metal incorporation preferences during calcite crystal growth, *Geochimica et Cosmochimica Acta* **66**, 3943-3954.

Fenter P., Geissbühler P., DiMasi E., Srajer G., Sorensen L.B., Sturchio N.C. (2000) Surface speciation of calcite observed *in situ* by high-resolution X-ray reflectivity, *Geochimica et Cosmochimica Acta* **64**, 1221-1228.

Freij S.J., Godelitsas A., Putnis A. (2005) Crystal growth and dissolution processes at the calcite-water interface in the presence of zinc ions, *Journal of Crystal Growth* **273**, 535-545.

Garcia B., Beaumont V., Perfetti E., Rouchon V., Blanchet D., Oger P., Dromart G., Huc A., Haeseler F. (2010) Experiments and geochemical modelling of CO_2 sequestration by olivine: Potential, quantification, *Applied Geochemistry* **25**, 1383-1396.

Glasner A., Weiss D. (1980) The crystallization of calcite from aqueous solutions and the role of zinc and magnesium ions - I. Precipitation of calcite in the presence of Zn^{2+} ions, *Journal of Inorganic and Nuclear Chemistry* **42**, 655-663.

Hillner P.E., Manne S., Gratz A.J., Hansma P.K. (1992) AFM images of dissolution and growth on a calcite crystal, *Ultramicroscopy* **42-44**, 2, 1387-1393.

IPCC (2005) Special Report on Carbon Capture and Storage.

Johnson J.W., Oelkers E.H., Helgeson H.C. (1992) SUPCRT92: A software package for calculating the standard molal thermodynamic properties of mineral, gases, aqueous species, and reactions from 1 to 5000 bar and 0 to 1000°C, *Computer & Geosciences* **18**, 899-947.

Kharaka Y.K., Cole D.R., Hovorka S.D., Gunter W.D., Knauss K.G., Freifield B.M. (2006) Gas-water-rock interactions in Frio Formation following CO_2 injection: Implications for the storage of greenhouse gases in sedimentary basins, *Geology* **34**, 577-580.

Kharaka Y.K., Thordsen J.J., Hovorka S.D., Nance H.S., Cole D.R., Phelps T.J., Knauss K.G. (2009) Potential environmental issues of CO_2 storage in deep saline aquifers: Geochemical results from the Frio-I Brine Pilot test, Texas, USA, *Applied Geochemistry* **24**, 1106-1112.

Lafargue E., Marquis F., Pillot D. (1998) Rock-Eval 6 Applications in Hydrocarbon Exploration, Production, and Soil Contamination Studies, *Revue de l'Institut Français du Pétrole* **53**, 421-437.

Lakshtanov L.Z., Stipp S.L.S. (2007) Experimental study of nickel (II) interaction with calcite: Adsorption and coprecipitation, *Geochimica et Cosmochimica Acta* **71**, 3686-3697.

Le Pape P., Ayrault S., Quantin C. (2012) Trace element behavior and partition *versus* urbanization gradient in an urban river (Orge River, France), *Journal of Hydrology* **472-473**, 99-110.

Little M.G., Jackson R.B. (2010) Potential impacts of leakage from deep CO_2 geosequestration on overlying freshwater aquifers, *Environmental Science and Technology* **44**, 9225-32.

Loisy C., Cohen G., Laveuf C., Le Roux O., Delaplace P., Magnier C., Rouchon V., Cerepi A., Garcia B. (2013) The CO_2-Vadose Project: Dynamics of the natural CO_2 in a carbonate vadose zone, *International Journal of Greenhouse Gas Control* **14**, 97-112.

Lorens R.B. (1981) Sr, Cd, Mn and Co distribution coefficients in calcite as a function of calcite precipitation rate, *Geochimica et Cosmochimica Acta* **45**, 553-561.

Martin-Garin A., van Cappellen P., Charlet L. (2003) Aqueous cadmium uptake by calcite: A stirred flow-through reactor study, *Geochimica et Cosmochimica Acta* **67**, 2763-2774.

Morris M.C., McMurdie H.F., Evans E.H., Paretzkin B., Parker H.S., Panagiotopoulos N.C. (1981) Standard X-ray Diffraction Powder Patterns, *NBS Monograph* **25**, Section 18.

Mucci A. (1986) Growth kinetics and composition of magnesian calcite overgrowths precipitated from seawater: Quantitative influence of orthophosphate ions, *Geochimica et Cosmochimica Acta* **50**, 2255-2265.

Parkhurst D.L., Appelo C.A.J. (1999) User's guide to PHREEQC (version 2) - A Computer Program for Speciation, Batch-Reaction, One-Dimensional Transport, and Inverse Geochemical Calculations.

Parkhurst D.L., Appelo C.A.J. (2013) Description of Input and Examples for PHREEQC Version 3 - A Computer Program for Speciation, Batch-Reaction, One-Dimensional Transport, and Inverse Geochemical Calculations.

Pauwels H., Gaus I., Le Nindre Y.M., Pearce J., Czernichowski-Lauriol I. (2007) Chemistry of fluids from a natural analogue for a geological CO_2 storage site (Montmiral, France): Lessons for CO_2-water-rock interaction assessment and monitoring, *Applied Geochemistry* **22**, 2817-2833.

Pérez del Villar L., Bruno J., Campos R., Gomez P., Cozar J.S., Garralon A., Buil B., Arcos D., Carretero G., Ruiz Sanchez-Porro J., Hernan P. (2002) The uranium ore from Mina Fe (Salamanca, Spain) as a natural analogue of processes in a spent fuel repository, *Chemical Geology* **190**, 395-415.

Pingitore N.E.J., Eastman M.P. (1984) The experimental partitioning of Ba^{2+} into calcite, *Chemical Geology* **45**, 113-120.

Pingitore N.E.J., Eastman M.P. (1986) The coprecipitation of Sr^{2+} with calcite at 25°C and 1 atm, *Geochimica et Cosmochimica Acta* **50**, 2195-2203.

Pingitore N.E.J., Eastman M.P., Sandidge M., Oden K., Freiha B. (1988) The coprecipitation of manganese(II) with calcite: an experimental study, *Marine Chemistry* **25**, 107-120.

Pokrovsky O.S., Mielczarski J.A., Barres O., Schott J. (2000) Surface Speciation Models of Calcite and Dolomite/Aqueous Solution Interfaces and Their Spectroscopic Evaluation, *Langmuir* **16**, 2677-2688.

Preis W., Gamsjäger H. (2001) (Solid + solute) phase equilibria in aqueous solution. XIII. Thermodynamic properties of hydrozincite and predominance diagrams for (Zn^{2+} + H_2O + CO_2), *Journal of Chemical Thermodynamics* **33**, 803-819.

Reeder R.J. (1983) Carbonates: Mineralogy and Chemistry, Mineralogical Society of America.

Reeder R.J. (1996) Interaction of divalent cobalt, zinc, cadmium, and barium with the calcite surface during layer growth, *Geochimica et Cosmochimica Acta* **60**, 1543-1552.

Smyth R.C., Hovorka S.D., Lu J., Romanak K.D., Partin J.W., Wong C., Yang C. (2009) Assessing risk to fresh water resources from long term CO_2 injection - laboratory and field studies, *Energy Procedia* **1**, 1957-1964.

Stipp S.L., Hochella M.F. (1991) Structure and bonding environments at the calcite surface as observed with X-ray photoelectron spectroscopy (XPS) and low energy electron diffraction (LEED), *Geochimica et Cosmochimica Acta* **55**, 1723-1736.

Stipp S.L.S. (1999) Toward a conceptual model of the calcite surface: Hydration, hydrolysis, and surface potential, *Geochimica et Cosmochimica Acta* **63**, 3121-3131.

Sverjensky D.A. (2003) Standard states for the activities of mineral surface sites and species, *Geochimica et Cosmochimica Acta* **67**, 17-28.

Swanson H.E., Fuyat R.K., Ugrinic G.M. (1954) NBS Circular 539, Vol. 3 - Data for 34 inorganic substances.

Tertre E., Beaucaire C., Juery A., Ly J. (2010) Methodology to obtain exchange properties of the calcite surface - Application to major and trace elements: Ca(II), HCO_3^-, and Zn(II), *Journal of Colloid and Interface Science* **347**, 120-126.

Tsusue A., Holland H.D. (1966) The coprecipitation of cations with $CaCO_3$ - III. The coprecipitation of Zn^{2+} with calcite between 50 and 250°C, *Geochimica et Cosmochimica Acta* **30**, 439-440.

Villegas-Jiménez A., Mucci A., Paquette J. (2009a) Proton/calcium ion exchange behavior of calcite, *Physical Chemistry Chemical Physics* **11**, 8895-8912.

Villegas-Jiménez A., Mucci A., Pokrovsky O.S., Schott J. (2009b) Defining reactive sites on hydrated mineral surfaces: Rhombohedral carbonate minerals, *Geochimica et Cosmochimica Acta* **73**, 4326-4345.

Viswanathan H., Dai Z., Lopano C., Keating E., Hakala J.A., Scheckel K.G., Zheng L., Guthrie G.D., Pawar R. (2012) Developing a robust geochemical and reactive transport model to evaluate possible sources of arsenic at the CO_2 sequestration natural analog site in Chimayo, New Mexico, *International Journal of Greenhouse Gas Control* **10**, 199-214.

Wright K., Cygan R.T., Slater B. (2001) Structure of the (10$\bar{1}$4) surfaces of calcite, dolomite and magnesite under wet and dry conditions, *Physical Chemistry Chemical Physics* **3**, 839-844.

Zachara J.M., Cowan C.E., Resch C.T. (1991) Sorption of divalent metals on calcite, *Geochimica et Cosmochimica Acta* **55**, 1549-1562.

Zachara J.M., Kittrick J.A., Harsh J.B. (1988) The mechanism of Zn^{2+} adsorption on calcite, *Geochimica et Cosmochimica Acta* **52**, 2281-2291.

Manuscript submitted in April 2015
Manuscript accepted in November 2015
Published online in April 2016

Cite this article as: B. Auffray, B. Garcia, C.-P Lienemann, L. Sorbier and A. Cerepi (2016). Zn(II), Mn(II) and Sr(II) Behavior in a Natural Carbonate Reservoir System., *Oil Gas Sci. Technol* **71**, 47.

APPENDIX

TABLE 1A

Impact of the database used for calculations of the $H_2O - CO_2 - CaCO_3$ system equilibrium in saline (100 g/L NaCl) conditions

Experiment ID	Minteq.v4.dat	Pitzer.dat	Minteq.v4.dat – pitzer.dat	
	Ca(II)eq (mol/L)	Ca(II)eq (mol/L)	Delta Ca(II) (mol/L)	% (relative to pitzer.dat)
4	1.15×10^{-3}	1.43×10^{-3}	-2.81×10^{-4}	−19.68
5	1.23×10^{-3}	1.49×10^{-3}	-2.63×10^{-4}	−17.66
6	1.27×10^{-3}	1.52×10^{-3}	-2.53×10^{-4}	−16.60
10	1.42×10^{-3}	1.63×10^{-3}	-2.16×10^{-4}	−13.23
11	1.48×10^{-3}	1.68×10^{-3}	-1.99×10^{-4}	−11.84
12	1.57×10^{-3}	1.75×10^{-3}	-1.75×10^{-4}	−10.02
16	1.15×10^{-3}	1.43×10^{-3}	-2.81×10^{-4}	−19.68
17	1.23×10^{-3}	1.49×10^{-3}	-2.63×10^{-4}	−17.66
18	1.19×10^{-3}	1.46×10^{-3}	-2.71×10^{-4}	−18.55
22	1.51×10^{-3}	1.70×10^{-3}	-1.93×10^{-4}	−11.34
23	1.69×10^{-3}	1.83×10^{-3}	-1.45×10^{-4}	−7.92
24	1.67×10^{-3}	1.82×10^{-3}	-1.49×10^{-4}	−8.18